Application Note

Potentiostat integration with AWS equipment

Summary

Seamless integration of QCMD and electrochemistry in the AWSensors EQCMD systems allows simultaneous measurements of the amount, electrochemical properties, and organization of material at the air/liquid interface accessed through the changes in the resonance frequency and dissipation measured by QCMD and the potential/current relationships measured with an integrated potentiostat or a galvanostat. The capabilities of the integrated AWSensors electrochemical EQCMD systems are illustrated here using the electropolymerization of aniline as an example.

Introduction

Investigation of complex interfacial processes benefit from combinations of complementary surface-analytical techniques that are based on different principles and approach the interface from complementary perspectives. [1,2] In this regard, the electrochemical quartz crystal microbalance (EQCM) with dissipation measurements, or EQCMD, has a venerable history.[3,4,5] Indeed, one of the incentives for immersing QCMD in liquids in the 1980s was to perform combined EQCMD measurements. [6] The two approaches are complementary in terms of the information they provide about the solid-liquid interface: interfacial mass transfer and structural changes are accessed with QCMD, while electrochemistry is concerned with the interfacial charge transfer and surface potential changes. Of particular interest is the quantitative characterization of electrochemically driven structural or viscoelastic transitions in interfacial layers, e.g., in battery research.[7]

To accommodate the needs of researchers working with electrochemical applications in a wide variety of fields, AWSensors developed QCMD instruments with integrated potentiostat/galvanostat control for synchronizing QCMD and electrochemical experiments with appropriate BioLogic potentiostat or galvanostat. To illustrate the functionality, we use a straight-forward aniline polymerization experiment.

Electropolymerization of aniline to form polyaniline (PANI), and its electrochemical properties, have been widely studied, including by electrochemical quartz crystal microbalance (ref. 8,9,10 and references therein). Here, we go through the necessary steps for setting up an electrochemical experiment with the integrated QCMD/potentiostat combination for following aniline electropolymerization on the gold electrode surface of a QCMD sensor. The gravimetric and electrochemical results are presented, and the gravimetric results are compared with the cyclic voltammetry.

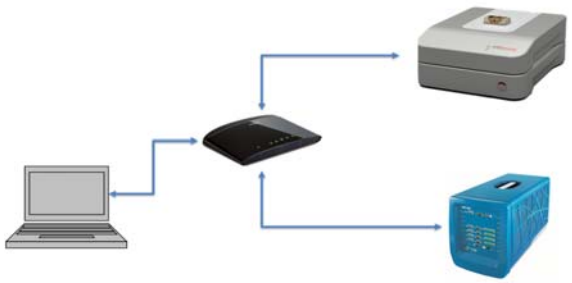

Figure 1: *AWSensors X1 QCMD (grey) / BioLogic potentiostat (blue) combination with the network connection diagram. The instruments are connected to a network switch (black) and controlled with the AWS Suite software.*

Experimental

QCMD

QCMD measurements were performed with the commercial X1 system (**Figure 1**) using an in-batch EQCM quick-lock cell for mounting standard AT-cut 5 MHz quartz crystal resonators (QCMD sensors) with polished gold electrodes (AWS SNS 000043 A).

The AWSensors EQCM cells (**Figure 2**) use the three-electrode configuration where the working electrode (WE) is the front electrode of the QCMD sensor that is grounded, the counter-electrode (CE), made out of a Platinum coil, and a Ag|AgCl (in 3M NaCl) reference electrode (RE). The counter and reference electrodes are normally supplied with the cell.

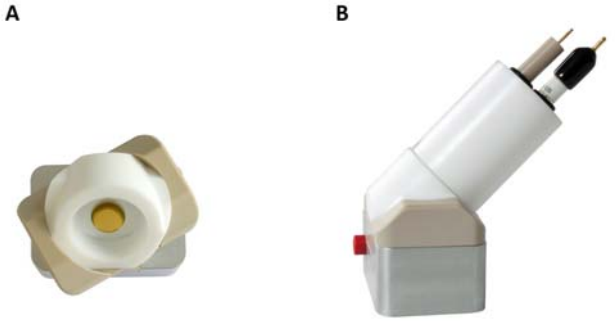

Figure 2: *An in-batch EQCM Quick-lock measurement cell. (A) with the electrode holder removed. (B) with the electrode holder assembled, viewed from the side. The electrode holder is used for mounting the reference electrode (black cap) and the counter electrode (grey). The working electrode connection (red), that connects to the sensor surface, is visible in the back of the measurement cell.*

Electrochemistry

A BioLogic SP-200 potentiostat/galvanostat was used which is compatible with AWSensors equipment and fully integrated into the control software. Please contact AWSensors regarding compatibility of other potentiostat models.

Equipment connection and configuration

Both instruments are connected via an Ethernet switch to a computer (**Figure 1**) running AWS Suite software that controls both the X1 and the potentiostat, which is included in the list of devices for the software to connect to (**Figure 3**).

On the hardware side, the appropriate leads of the Ultra-Low current cable of the SP-200 potentiostat were connected to the relevant electrodes of the EQCM cell in the "WE to ground" connection mode depicted in the screenshot from the AWS Suite software (**Figure 4**).

The Potentiostat is automatically configured for floating mode operation (WE to ground) when a connection is set up in the AWS Suite; no user intervention is needed. It is important, however, that the potentiostat cable is connected to the EQCM **after** the user has connected the

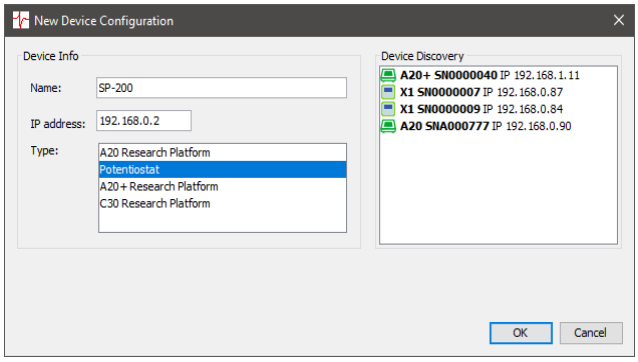

Figure 3: *Potentiostat device selection in the AWS Suite. AWS Suite software recognizes compatible potentiostats connected to the network.*

software to the Potentiostat device to avoid power surges at the electrodes.

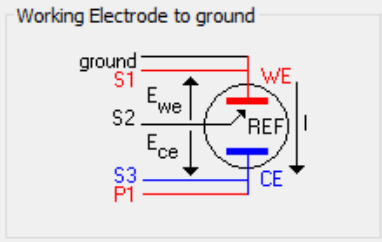

Figure 4: *Working Electrode (WE) to ground connection mode.*

Once the appropriate software configuration and hardware connections are made, an EQCMD experiment can be created (**Figure 5**) and configured (**Figure 6**).

Configuring and running an EQCMD experiment: electrochemical polymerization of aniline

For performing an EQCM experiment, a QCMD sensor was installed in the cell. After the reference and the counter electrodes were inserted into the chimney of the cell, the cell was filled with ~ 10 ml of the 0.030 M aniline solution in 1.0 M $HClO_4$. A new experiment with the potentiostat enabled was created in AWS Suite (**Figure 5**). QCMD parameters were configured as shown in **Figure 6A** and the electrochemical parameters were configured as shown in **Figure 6B**. For the QCMD, the relevant configuration parameters are the type of the sensor and the overtones, on which the resonance frequency and dissipation signals are to be recorded (n = 1 to n = 13 in **Figure 6A**). The relevant configuration parameters for the electrochemical part of the experiment include the type of data recorded and the current/potential ranges (Cyclic Voltammetry with the potential spanning − 0.1 and 1.1 V at rate of 50 mV/s). QCMD and the current/voltage signals are both stored in the same file and can be presented in various ways in the AWS Suite software, as shown below in the **Results** section.

Results

EQCMD signal response

The results of the EQCMD experiment are shown in **Figure 7** and **Figure 8**. **Figure 7** shows the evolution of the signals (potential, current, normalized frequency and dissipation shifts) as a function of time. As the potential applied to the surface is cycled between – 0.1 and + 1.1 V, the current responds with cyclical changes that, apart from the initial spike, grow in amplitude and develop a fine structure.

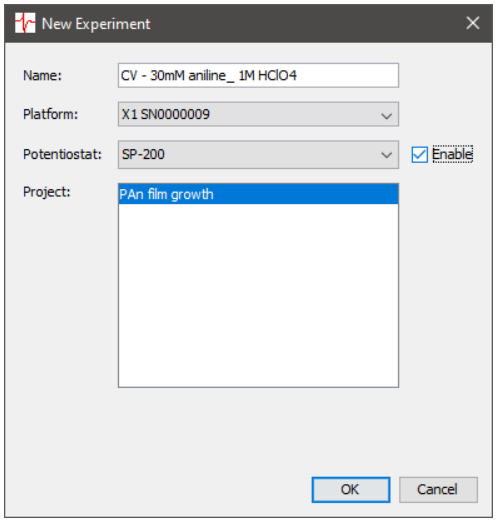

Figure 5: *New experiment creation window in AWS Suite.*

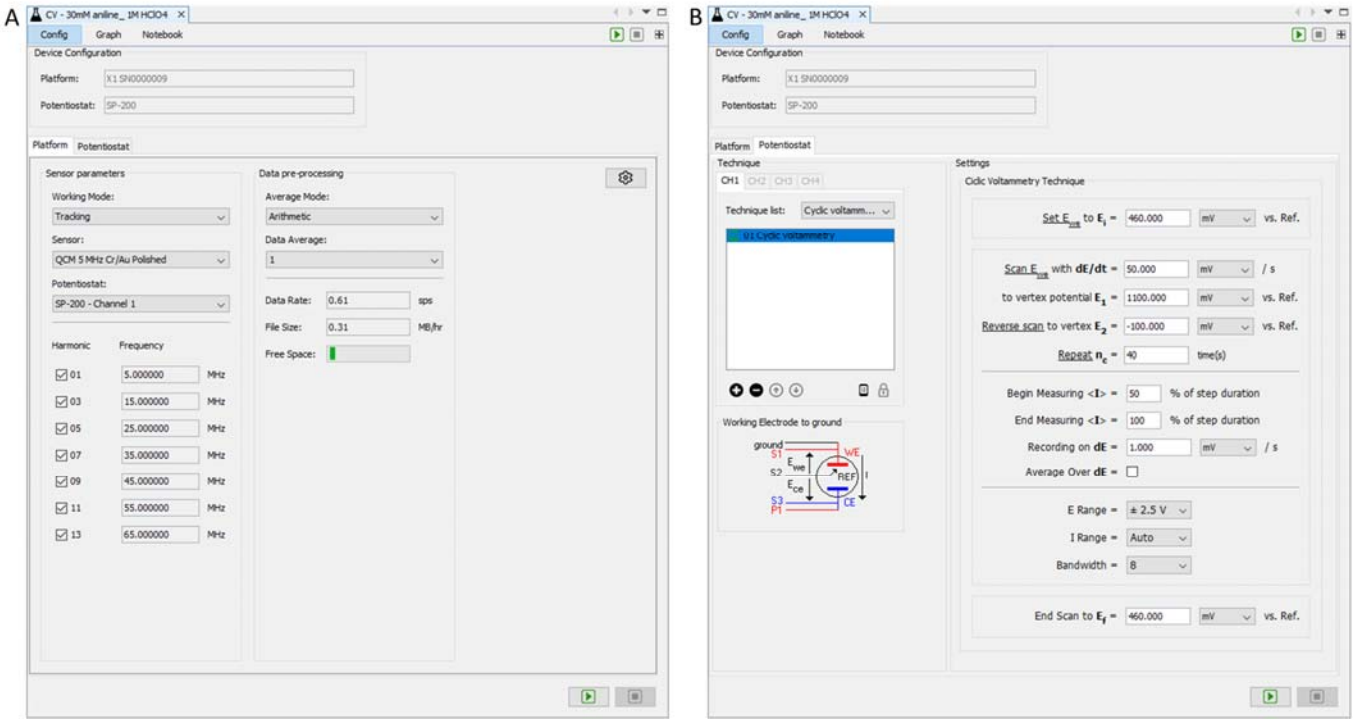

Figure 6: *Experiment configuration in the AWS Suite. The parameters related to the QCMD measurement (sensor type, number of harmonics...) are selected in the Platform tab (A). The electrochemical techniques to be applied are configured in the Potentiostat tab (B).*

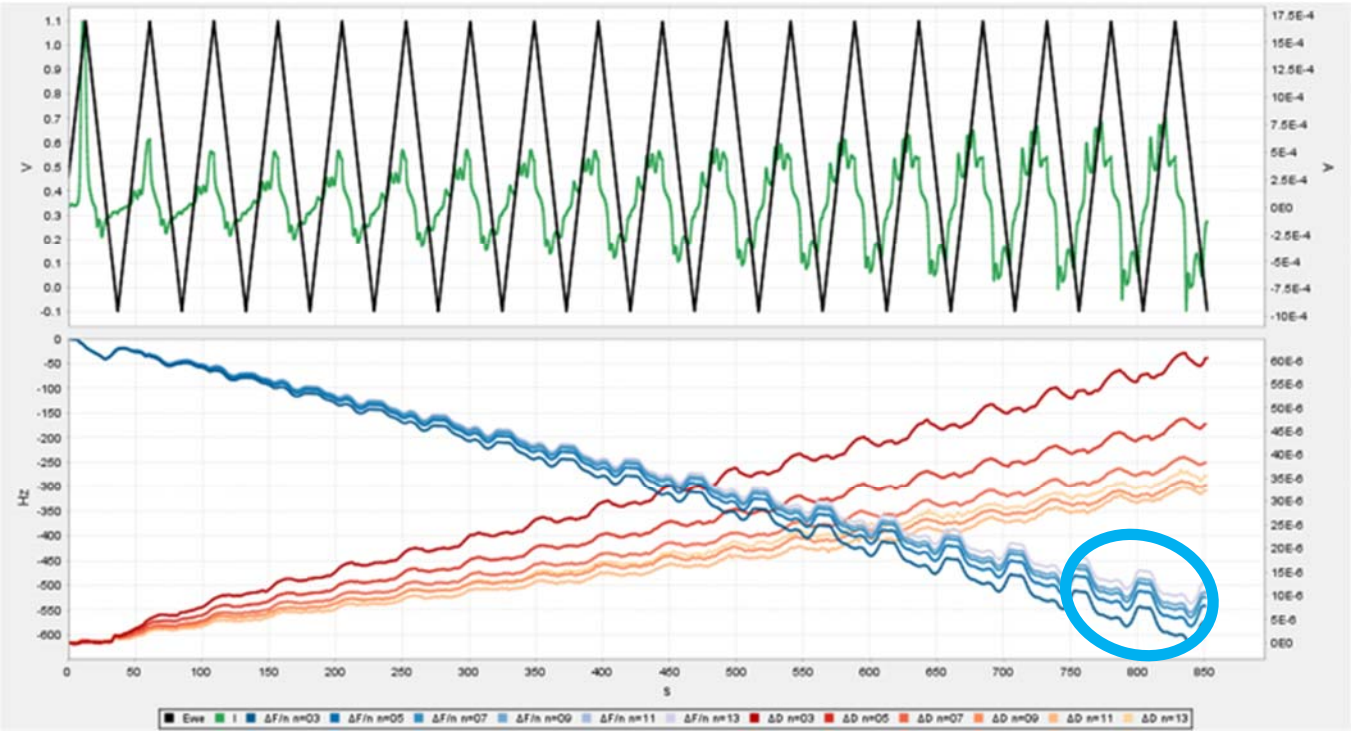

Figure 7: *PANI film formation in a solution containing 0.030 M aniline and 1.0 M HClO4 at a scan rate of 50 mV/s. Time-dependence of the working electrode potential (Ewe, black), current (I, green) are plotted on the top panel. Normalized frequency shift shifts, ΔF/n, and dissipation shifts, ΔD, for the different overtones, n, are plotted in the bottom panel. Light blue circle highlights the small potential-dependent cyclical variations of the frequency.*

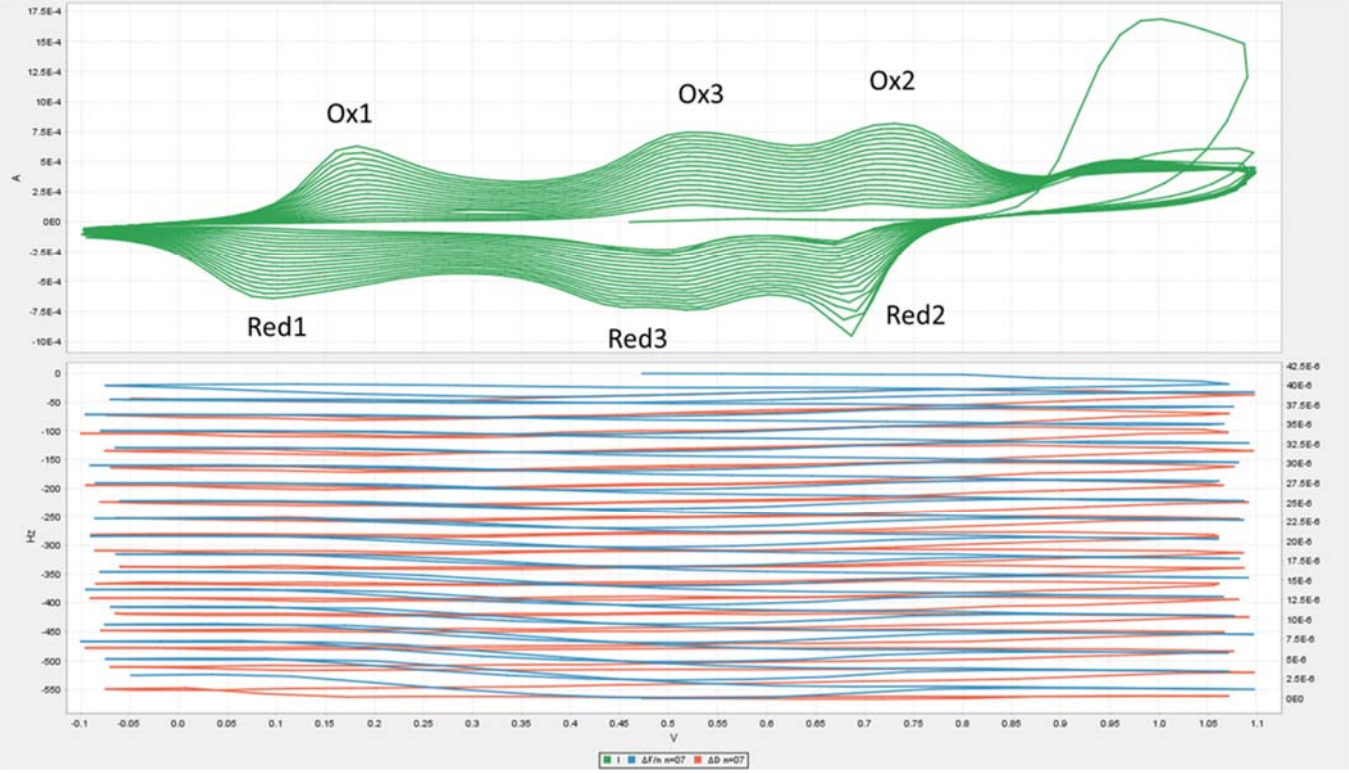

Figure 8: *PANI film in a solution containing 0.030 M aniline and 1.0 M $HClO_4$ at a scan rate of 50 mV/s. Same data as in Figure 7, but plotted as a function of the working electrode potential, Ewe. The cyclic voltammograms (current vs. voltage, CV) are shown in the top plot, and the corresponding frequency and dissipation shifts for the 7th overtone are plotted in the bottom one. Note that data was recorded for all 18 potential cycles. Only one overtone is selected for clarity in this plot, but data for all overtones is available in the software, to be selected by the user. Peaks in the CV curves are labeled after ref. 9.*

.

AWSensors Scientific Technology

p:+34 961 336 899 | www.awsensors.com | awsensors@awsensors.com

At the same time, the frequency decreases, indicating a net deposition of mass on the sensor surface, while the dissipation increases, indicating that the resulting film is "lossy" (viscoelastic). This is also supported by the increasing overtone dispersion: the differences between the signals from the different overtones increase with the number of cycles. This is expected for the growth of a viscoelastic film and it is one of the reasons that multiple-harmonic analysis is useful for detecting viscoelastic behavior. Both the frequency and the dissipation signals also undergo smaller, cyclical variations on the background of these overall trends (highlighted with a light blue circle in **Figure 7**).

In **Figure 8**, the same data are presented as a function of potential. This form of presenting the data reveals the classical appearance of the cyclic voltammogram, from which potential-specific current peaks can be read off and oxidation processes determined.[10] Here, it is worth highlighting that the first CV cycle appears rather different from the subsequent ones, due to the changes at the gold/liquid interface with the polymer deposition. The process of the polymer (PANI) growth at the surface can be inferred from the steady decrease in the frequency with the number of cycles.

Also, as the film grows, the anion insertion and release are becoming increasingly important. These processes cause the increase in the amplitude of the current changes registered at the working electrode with the number of cycles visible in both **Figure 7** and **Figure 8**, as well as the cyclical changes in the frequency and dissipation shifts noted above (highlighted in **Figure 7**); these occur at the potential of 0.2V, which corresponds to the anion insertion due to the p-doping of the polymer. The net mass increase for each cycle is almost constant, as observed in **Figure 8**, indicating that the growth rate remains constant regardless of the amount of polymer accumulated on the electrode surface.

Finally, we show in **Figure 9** how the sensor looks before and after the polymerization: a green polymer film has formed on the surface of the gold sensor after the polymerization. The film can be removed using, e.g., the piranha treatment, and the cleaned sensor can be reused.

Figure 9: *A QCMD sensor before and after the aniline polymerization.*

Data analysis

The frequency shifts, plotted in **Figure 7**, can be converted into areal mass density via the Sauerbrey relationship,[11] $m_f \approx -\frac{\Delta f Z_q}{2nf^2}$, where m_f is the areal mass density, Δf is the frequency shift, Z_q is the acoustic impedance of the AT-cut quartz (8.39E+06 Ns/m^3), n is the overtone order, and f is the fundamental resonance frequency of the sensor (5 MHz). The results are plotted in **Figure 10**, revealing a paradox: the Sauerbrey mass appears different on the different overtones; that, of course, is physically impossible: the mass of the layer must be independent of the frequency, at which it is measured.

The paradox is resolved by realizing that the overtone dispersion arises from the viscoelastic properties of the layer. They can be accurately captured by a model that represents the mechanical response of the layer in terms of frequency-dependent shear-elastic compliance (the inverse of the shear elastic modulus), $\tilde{J}_f(f)$, defined as $\tilde{J}_f(f) = J'_f\left(\frac{f}{f_{ref}}\right)^{\beta'} - iJ''_f\left(\frac{f}{f_{ref}}\right)^{\beta''}$, where the real and imaginary parts refer to the elastic and viscous compliances, respectively, and the frequency dependence of each of them is captured through the power-law dependence with the two exponents, β' and

β"; f_{ref} is an arbitrary reference frequency (30 MHz in this case), and f is the measurement frequency.

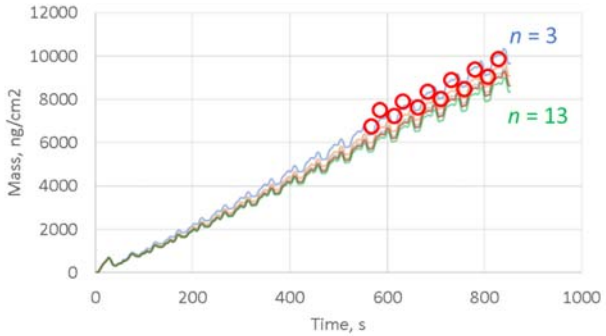

Figure 10: *Data analysis. The frequency data shown in* ***Error! Reference source not found.*** *are converted into Sauerbrey mass for each overtone independently (lines) and plotted here together with the results of the fit to the viscoelastic model (red circles) that combines the frequency and dissipation data from the different overtones.*

The frequency and dissipation response of a viscoelastic layer is then

$\Delta\tilde{f} \approx -\frac{2f^2 m_f}{Z_q}\left(1 - i2\pi f n \frac{\tilde{J}_f(f)}{\varrho_f}\varrho_{liq}\eta_{liq}\right)$,[2] where the complex frequency shift $\Delta\tilde{f} = \Delta f + i\Delta\Gamma$, with the bandwidth $\Gamma = Df/2$, consists of a Sauerbrey mass and a viscoelastic correction; note, that the bulk liquid properties, density and viscosity $\varrho_{liq}\eta_{liq}$, enter the viscoelastic correction term.

The frequency and dissipation data shown in **Figure 7** were fitted with five parameters: m_f, J', $J"$, β', and $\beta"$. The fitting was done using freely available software (QTM).[12]

The mass that was obtained from the fit is shown in **Figure 10** (red circles). Note, how it is now independent of the measurement frequency (overtone order), as it should be. Note also, that the cyclical variations that were observed in the in the frequency shifts (**Figure 7**) are still visible here in the fitted mass. These cyclical mass changes originate from the anion insertion that causes the swelling of the film to depend on the applied potential.

The mass that is obtained from the fitting is similar to that reported in ref. 9.

It is instructive to examine the behavior the viscous and the elastic compliances; they are shown in **Figure 11**. Over the period of time chosen for the fit, the exponents, β' and $\beta"$, were approximately constant at -2.2 ± 0.6 and -0.6 ± 0.1, respectively.

In order to put the values of the compliances and the exponents in perspective –

- The viscosity of water, $\tilde{\eta} = \eta' - i\eta"$, is η' = 1 mPa*s, $\eta"$ = 0; both exponents are zero. Converting this into $\tilde{J}_f$ using $\tilde{\eta} = \frac{1}{i\omega\tilde{J}}$ (see eq.4.1.6 in ref. 2) yields J' = 0 and β' = 0, $J"$ = 5.3 1/MPa, and $\beta"$ = – 1. In general, it is expected that – 2 < β' < 0 and – 1 < $\beta"$ < 1.[2]
- Certain surface-anchored poly(amino acid) repeats in water yield J'~ 1.5 1/MPa, $J"$ ~ 2.5 1/MPa, β'~ –1.3, and $\beta"$~ – 0.5.[13]
- On the other hand, in the stiff polymers cross-linked by UV curing, J' and $J"$ tend to very small values of 0.001 and 0.00005 1/MPa, respectively, with β' and $\beta"$~ – 0.4.[14]

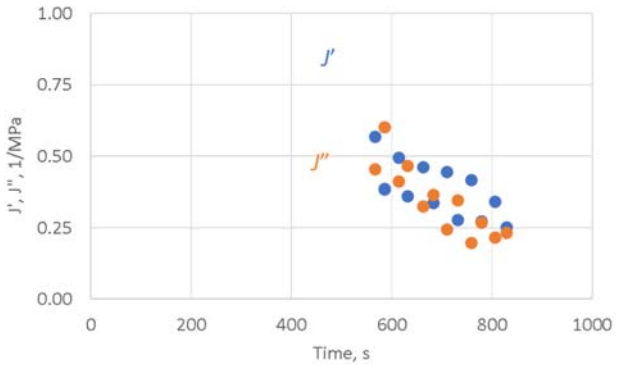

Figure 11: *Elastic and viscos compliances corresponding to the fit results shown in Figure 10.*

AWSensors Scientific Technology

p:+34 961 336 899 | www.awsensors.com | awsensors@awsensors.com

Conclusions

This *Application Note* is intended as a guide for performing EQCMD experiments with the AWSensors instrumentation. The capabilities of AWSensors instruments and software for integrated electrochemical and QCMD measurements is demonstrated using electropolymerization of aniline as an example. Setup of the QCMD and electrochemical aspects of the experiments in the integrated software module is explained. Typical results are presented. Their analysis and fitting of the data to the viscoelastic module is discussed.

Remarks

- The AWSensors X1 QCMD system monitors frequency and dissipation shifts at multiple harmonics.
- AWSensors instruments, including the X1, are easily adaptable to perform EQCMD experiments via use of quick-lock QCM cells, designed for this very purpose.
- Configuration and operation of both QCMD and Potentiostat equipment, as well as, signal synchronization is completely integrated within the AWS Suite, which greatly simplifies performing EQCMD experiments.

Tips!

1. When mounting the electrochemical cell, make sure that no bubbles are trapped in the sensor surface. It is recommended to carefully deposit the electrolyte solution over the sensor surface and then introduce the electrode holder (cylinder) to finish filling the EQCM cell.
2. Place the reference electrode in the EQCM cell to finish filling it, in order to avoid possible liquid overflow.
3. Connect to the Potentiostat (via AWS Suite software) before connecting the electrometer cables to the EQCM cell electrodes.
4. Working at stable and well-controlled temperature is paramount for avoiding drifts. For the X1, using the Temperature Control Unit module is advised. This will also allow you to set the EQCM cell temperature slightly below room temperature to avoid outgassing (bubble formation).

AWSensors Scientific Technology

p:+34 961 336 899 | www.awsensors.com | awsensors@awsensors.com

Order Information

Product	Quantity	Reference
AWS X1	1	AWS X1 000031 A
X1 Temperature Control Unit	1	AWS X1 000032 A
EQCM in-batch cell for 14mm QCM	1	AWS CLS+ 000016 Q
QCM sensor, 14 mm, 5 MHz, Ti/Au, Polished	10	AWS SNS 000043 A

References

[1] Ernesto Calvo, Kay Kanazawa, Hubert Perrot, and Yolanda Jimenez, *Combination of Quartz Crystal Microbalance with other Techniques,* in Piezoelectric Transducers and Applications, A.A. Vives (ed.), 2008, doi: 10.1007/978-3-540-77508-9_13, Springer-Verlag Berlin Heidelberg.

[2] Johannsmann D. *The Quartz Crystal Microbalance in Soft Matter Research: Fundamentals and Modeling*. Springer International Publishing, 2015.

[3] Marx, KA *Quartz crystal microbalance: A useful tool for studying thin polymer films and complex biomolecular systems at the solution-surface interface* 2003, Biomacromolecules 4(5), 1099-1120, 10.1021/bm020116i.

[4] Buttry, DA., Ward, MD., *Measurement of interfacial processes at electrode surfaces with the electrochemical quartz crystal microbalance* 1992, *Chemical Reviews* 92(6), 1355-1379. 10.1021/cr00014a006

[5] Schumacher, R, *The quartz microbalance - a novel-approach to the in-situ investigation of interfacial phenomena at the solid liquid junction* 1990, *Angewandte Chemie-International Edition* 29(4), 329-343. 10.1002/anie.199003293

[6] Bruckenstein, S., Shay, M. *Experimental Aspects Of Use Of The Quartz Crystal Microbalance In Solution* 1985, *Electrochimica Acta* 30(10),1295-1300. doi: 10.1016/0013-4686(85)85005-2.

[7] Sigalov S. Electrochemical Quartz Crystal Microbalance with Dissipation Real- Time Hydrodynamic Spectroscopy of Porous Solids in Contact with Liquids. 2016, Anal. Chem. 88, 10151 – 10157.

[8] Cui, S. Y., & Park, S. M. (1999). *Electrochemistry of conductive polymers XXIII: polyaniline growth studied by electrochemical quartz crystal microbalance measurements*. Synthetic metals, 105(2), 91-98.

[9] Baba, A., Tian, S., Stefani, F., Xia, C., Wang, Z., Advincula, R. C., ... & Knoll, W. (2004). *Electropolymerization and doping/dedoping properties of polyaniline thin films as studied by electrochemical-surface plasmon spectroscopy and by the quartz crystal microbalance*. Journal of Electroanalytical Chemistry, 562(1), 95-103.

[10] Xie et al. *Electrochemical Quartz Crystal Microbalance Monitoring of the Cyclic Voltammetric Deposition of Polyaniline: A Laboratory Experiment for Undergraduates*. 2007, *Journal of Chemical Education* 84(4), 681 – 684.

[11] Sauerbrey, G., *Verwendung von Schwingquarzen zur Wägung Dünner Schichten und zur Mikrowägung,* 1959. *Zeitschrift für Physik* 155(2), 206-222.

[12] https://www.pc.tu-clausthal.de/en/research/qcm-modelling/ , accessed 22.02.2021

[13] Eisele N.B. *Viscoelasticity of Thin Biomolecular Films: A Case Study on Nucleoporin Phenylalanine-Glycine Repeats Grafted to a Histidine-Tag Capturing QCM-D Sensor*, 2012, Biomacromolecules 13(8):2322-32.doi: 10.1021/bm300577s

[14] Petri, J. *Determination of the Shear Modulus of Thin Polymer Films with a Quartz Crystal Microbalance: Application to UV-Curing*, 2019, Anal.Chem. 91, 1595−1602.